# High-density stable glasses formed on soft substrates

Peng Luo,<sup>1</sup> Sarah E. Wolf,<sup>2</sup> Shivajee Govind,<sup>1</sup> Richard B. Stephens,<sup>1</sup> Dong Hyup Kim,<sup>1,3</sup> Cindy Y. Chen,<sup>1</sup> Truc Nguyen,<sup>1</sup> Patryk Wąsik,<sup>4</sup> Mikhail Zhernenkov,<sup>4</sup> Brandon Mcclimon,<sup>5</sup> and Zahra Fakhraai<sup>1, a)</sup>

- <sup>1)</sup>Department of Chemistry, University of Pennsylvania, Philadelphia, Pennsylvania, 19104, USA
- <sup>2)</sup>Department of Chemistry, State University of New York Cortland, Cortland, New York, 13045, USA
- <sup>3)</sup>School of Chemical and Biological Engineering, Seoul National University, Seoul 08826, Republic of Korea
- <sup>4)</sup>National Synchrotron Light Source II (NSLS-II), Brookhaven National Laboratory, Upton, New York, 11973, USA
- <sup>5)</sup>Department of Mechanical Engineering & Applied Mechanics, University of Pennsylvania, Philadelphia, Pennsylvania, 19104, USA

**Abstract:** Physical vapor deposition can create high-density stable glasses comparable to liquid-quenched glasses aged for millions of years, enabled by surface-mediated equilibration. Deposition is often performed on rigid substrates, at various rates and temperatures, to control glass properties. Here, we demonstrate that on soft, rubbery substrates, surface-mediated equilibration is enhanced up to 170 nm away from the interface, forming stable glasses with densities up to 2.5% higher than liquid-quenched glasses, within 2.5 hours of deposition. To gain these properties on rigid substrates requires 10 million times slower deposition, taking  $\sim 3000$  years. Controlling the modulus of the rubbery substrate provides a large degree of control over the glass structure and density at a constant deposition condition. These results underscore the significance of substrate elasticity as a novel factor in manipulating the properties of the mobile surface layer and thus the vapor-deposited glass structure and properties, allowing access to deeper states of the energy landscape, without the need for prohibitively slow deposition rates.

Keywords: stable glass, physical vapor deposition, surface-mediated equilibration, structural anisotropy, glass transition, enhanced surface mobility

<sup>&</sup>lt;sup>a)</sup>Corresponding Author: fakhraai@sas.upenn.edu

Taking advantage of enhanced surface mobility<sup>1-6</sup>, a glass film grown through physical vapor deposition (PVD) onto a substrate held below the glass transition temperature  $(T_g)$  can explore more stable configurations and adopt unique structures that originate at the free surface<sup>7–12</sup>. Surfacemediated equilibration (SME) enables an extraordinary degree of tunability in the molecular orientation, packing structure, and stability of PVD glasses, through variations of the deposition rate  $(R_{dep})$  and substrate temperature  $(T_{dep})^{8,11,13-19}$ . Under deposition conditions where surface mobility is sufficiently fast and equilibration occurs well below the immediate surface 12 (typically  $T_{dep} \ge 0.9T_g$ ), isotropic packings are produced<sup>11,20</sup>, with thermodynamic stability analogous to those of liquid-quenched glasses (LQGs) aged for millions of years<sup>21</sup>. At lower  $T_{dep}$ 's, kinetically trapped stable glasses (SGs) with preferred molecular orientation<sup>8,11,14,22,23</sup>, or layered structures 11,22,24,25 are produced, allowing an exceptional degree of control over the mechanical<sup>13,16,18,26,27</sup>, optoelectronic<sup>17,28</sup>, and low-temperature properties<sup>29,30</sup> of SGs. While lowering  $R_{dep}$  can improve the stability and reduce the anisotropy at lower  $T_{dep}$ 's 15,16,20,21,23,31,32 (10 times decrease in  $R_{dep}$  is analogous to a  $\sim$ 17 K increase in  $T_{dep}$ , ref.<sup>23</sup>), it is typically difficult to do so within a reasonable experimental duration. Typical range of  $R_{dep}$  in high-vacuum chambers is 0.1 - 20 Å/s (ref.  $^{15,23}$ ) and can be reduced to 0.02 Å/s for volatile, low- $T_g$  molecules  $^{31}$ .

To form SGs, PVD is typically performed on rigid substrates. It remains an open question whether the rigidity of the interface can control aspects of the SG formation, through the nucleation of stable states or slowdown of the free surface mobility due to the influence of the substrate. In liquid-quenched polymer glasses, a subtle decrease in surface mobility was observed for films as thick as  $\simeq 180$  nm on silicon<sup>33</sup>. Roth and coworkers reported dramatic  $T_g$ -reduction over distances up to  $\approx 250$  nm on soft interfaces, indicating substantially enhanced and dynamically coupled mobility across the interface<sup>34,35</sup>. In PVD glasses, modification in the glass structure was only observed over a narrow range of just a few nanometers away from a rigid substrate<sup>36</sup> or an SG with higher  $T_g$  (ref.<sup>37,38</sup>) with no similar studies on soft substrates, to our knowledge. PVD on a soft substrate can elucidate whether substrate rigidity is critical in SG formation and reveal its length scale of influence.

Here, we deposit N,N'-Bis(3-methylphenyl)-N,N'-diphenylbenzidine (TPD) glasses (Young's modulus  $E \approx 7$  GPa, ref.<sup>39</sup>) on polydimethylsiloxane (PDMS) rubber films with various degrees of curing (soft substrates,  $E \approx 2.5 - 5.5$  MPa, see **Supplementary Note 1** and **Figure S1**) and compare their stability with TPD glasses deposited on silicon (rigid substrates,  $E \approx 75$  GPa, ref.<sup>35</sup>). We demonstrate that glasses produced on soft substrates are denser and more isotropic than those

deposited on rigid substrates, indicating their rate of surface equilibration is accelerated by 5-7 decades compared to those deposited on silicon and by more than 12-14 decades compared to bulk LQG<sup>21</sup>. To slowly deposit a glass with the same density and thickness on silicon,  $\sim$ 3000 years of time is required at the optimal  $T_{dep}$ . The enhanced rate of equilibration persists at distances up to  $\sim$ 170 nm away from the soft interface and can be controlled over a broad range of values through small changes of the PDMS modulus or thickness.

PDMS films with various thicknesses, curing temperatures, and washing conditions were prepared on silicon substrates. The surface morphology and roughness of these films were measured to be < 1 nm, (similar to the silicon substrates, **Figure S2**) and invariant of temperature (**Figure S3**). More details can be found in **Methods** and **Supplementary Information**. TPD ( $T_g = 331 \pm 1$  K) films (typically 180 nm thick) were deposited over a broad  $T_{dep}$ -range and  $R_{dep}$ 's of  $2 \pm 0.2$  Å/s and  $0.2 \pm 0.03$  Å/s on PDMS (typically 5 nm thick, cured at 383 K for 1 h,  $E = 4.8 \pm 0.3$  MPa, **Figure S1**) and bare silicon substrates. Variable angle spectroscopic ellipsometry (VASE), grazing-incidence wide-angle X-ray scattering (GIWAXS), and atomic force microscopy (AFM) were used to characterize the thermodynamic stability, anisotropic structure, and surface morphology of these films.

# **Enhanced Surface mobility and stability**

Compared to glasses deposited on silicon, which are smooth (**Figure S4**), those deposited on 5 nm thick PDMS films show larger root-mean-square roughness (RMS) with spinodal morphology (**Figures 1a,S5&S6**). On rigid substrates, similar surface morphology has only been observed in thin films ( $\lesssim 20$  nm) deposited at  $T_{dep}$ 's close to  $T_g$  (ref.<sup>40,41</sup>), where the entire film had enhanced mobility<sup>5,40</sup>. These observations suggest additional mobility enhancement on PDMS compared to silicon, which leads to stronger pattern formation. On 13 nm thick PDMS films with lower Young's moduli ( $E = 2.8 \pm 0.2$  MPa, **Figure S1**), the PVD film roughness is further increased (**Figure S7**), showing the strong role of the PDMS mechanical properties as opposed to a change in surface energy compared to silicon in enhancing the interfacial dynamics. Upon pre-heating briefly to just above  $T_g$  ( $T_g + 4$  K=335 K, **Figure 1d**), the RMS roughness is significantly reduced (**Figure 1b,c**), with an increase in the lateral correlation length ( $L_{corr}$ , **Figure S8**). We note that at this temperature bulk transformation of TPD SGs is expected to be exceedingly slow ( $\sim 10^{-3}$  nm/s transformation rate)<sup>42</sup>. As such, the high initial roughness and its rapid change upon preheating indicate that the surface layer has reduced  $T_g$  and enhanced mobility compared to the bulk. Both

the RMS roughness and  $L_{corr}$  of the morphology of as-deposited samples increase with increasing  $T_{dep}$  and decreasing  $R_{dep}$  (**Figures 1b,c&S8**), indicating the increasing thickness of the mobile surface layer with temperature, consistent with previous observations in polymeric and other glass surfaces on silicon<sup>43,44</sup>. However, the thickness of this layer appears to be significantly larger on PDMS compared to silicon.

*In-situ* spectroscopic ellipsometry (SE) measurements also reveal a noticeable change in the average refractive index ( $\langle n \rangle$ ) upon pre-heating of films deposited on PDMS ( $\delta \langle n \rangle = \langle n \rangle_{as-deposited}$  –  $\langle n \rangle_{pre-heated}$ ). As seen in **Figure 1d**, the transformation of the interfacial regions starts at ~317 K, reaching a plateau at  $T_g$  (see more data in Figures S9-S11). The bulk transformation of the film (red data in **Figure 1d**) occurs only after the film is heated to well above  $T_g$  with an onset at  $T_g + 18 \text{ K} = 349 \text{ K}$ , resulting in an apparent two-step transformation and decoupling of dynamics when pre-heating is not performed (Figure S12). In contrast, films deposited on silicon do not show any significant change in  $\langle n \rangle$  until heated to above the bulk transformation onset (**Figures S13&S14**). Unlike the surface roughness,  $\delta\langle n\rangle$  has a non-monotonic dependence on  $T_{dep}$ and becomes negligible at low  $T_{dep}$ 's (Figures 1e&S10). These observations suggest that the interfacial regions of the as-deposited films have improved thermodynamic stability, where the non-monotonic  $T_{dep}$ -dependence arises from an interplay between decreasing interfacial mobility and increasing driving force to equilibrium as  $T_{dep}$  is decreased, analogous to bulk SGs<sup>12</sup>. However, the onset temperature of transformation ( $\sim$ 317 $\pm$ 2 K) for these regions is well below the bulk onset ( $\sim$ 349 K for data in **Figures 1d&S12**). This is further evidence for the lower  $T_g$  value of the interfacial regions of films deposited on PDMS, with  $T_g$  similar to that of 10-20 nm films deposited on silicon<sup>5</sup>. While it is not clear which interface participates more strongly in the measured  $\delta \langle n \rangle$ , the roughness flattening provides direct evidence of the faster mobility at the free surface, influenced by the PDMS substrate  $\sim$ 180 nm away.

Surprisingly, once the glass is transformed to LQG only one  $T_g$  is observed with the same value and transition breadth as bulk TPD and TPD deposited on silicon (**Figure S15**), meaning that the dynamics are more uniform across the LQG films, unlike what had been previously observed in polymers on PDMS<sup>35</sup>. Recent simulations have shown that the surface mobility gradients can be strongly influenced by the degree of stability, leading to a decoupling of mobility in the most stable films<sup>11</sup>, providing a potential explanation for these observations.

# Enhanced bulk glass stability

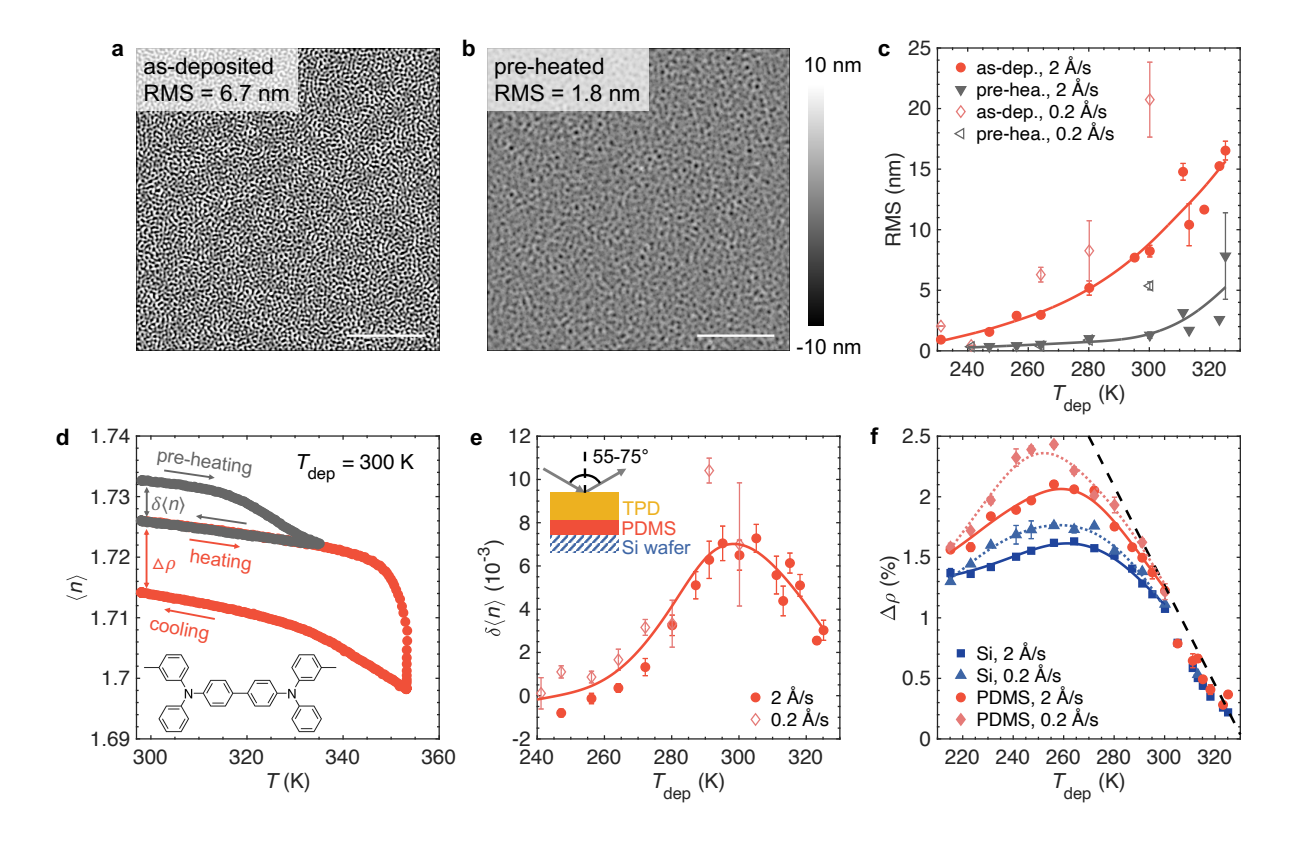


Figure 1. Surface morphology and thermodynamic stability of TPD glasses deposited on 5 nm PDMS and silicon substrates. a,b, AFM images of a film (a) as-deposited at  $R_{dep}=2$  Å/s and  $T_{dep}=300$  K and (b) after pre-heating with thermal protocol shown in (d). Scale bars, 5  $\mu$ m. c, RMS roughness of as-deposited (red) and pre-heated (gray) films vs.  $T_{dep}$  at two different  $R_{dep}$ 's. d,  $\langle n \rangle$  vs. temperature during dilatometry cycles at heating/cooling rates of 10 K/min for a film deposited at  $T_{dep}=300$  K and  $R_{dep}=2$  Å/s. The arrows denote the direction of the thermal cycling. The film is pre-heated to 335 K and immediately cooled back to 298 K (gray circles) to measure  $\delta\langle n \rangle$ , then heated to 353 K for bulk transformation and cooled back to 298 K (red circles) to measure  $\Delta \rho$ . Inset: chemical structure of the TPD molecule. e,  $\delta\langle n \rangle$  vs.  $T_{dep}$  for films deposited at  $R_{dep}=2$  Å/s (filled circles) and  $R_{dep}=0.2$  Å/s (open diamonds). Inset: schematic geometry of VASE measurements. f,  $\Delta \rho$  vs.  $T_{dep}$  for films deposited on PDMS (red) and silicon (blue) at two different  $R_{dep}$ 's. The solid and dotted lines in (c,e,f) serve as guides for the eyes, and the dashed line in (f) represents the extrapolated value for the SCL (Figure S15). Where not seen, the error bars (standard error) are smaller than the symbol size.

To evaluate the bulk glass stability on PDMS, the change in density  $(\Delta \rho)$  was calculated based on the change in  $\langle n \rangle$  upon the thermal transformation (**Figure 1d**) of pre-heated (or as-deposited,

depending on the initial film roughness as detailed in **Methods**) films, using the Lorentz-Lorenz equation<sup>45</sup> (see **Methods**, **Supplementary Note 2** and **Figure S16**).

**Figure 1f** shows that glasses deposited on PDMS have a higher relative density than those on silicon. These differences are larger if pre-heating is not performed (**Figure S17**). SGs made on PDMS follow the extrapolated SCL values (dashed line in **Figure 1f**) down to lower temperatures ( $T_{dep} \sim 290 \text{ K}$ , *i.e.*  $0.88T_g$  vs.  $T_{dep} \sim 300 \text{ K}$ , *i.e.*,  $0.91T_g$  on silicon), and reach a higher maximum  $\Delta \rho$ . At  $T_{dep} \approx 255 \text{ K}$  and  $R_{dep} = 2 \text{ Å/s}$ ,  $\Delta \rho \approx 2.1\%$  on PDMS vs.  $\approx 1.6\%$  on silicon. At  $R_{dep} = 0.2 \text{ Å/s}$ ,  $\Delta \rho$  increases more dramatically on PDMS ( $\approx 2.4\%$  vs.  $\approx 1.7\%$  on silicon). To achieve  $\Delta \rho \sim 2.1\%$  and  $\Delta \rho \sim 2.4\%$  on silicon, even at the optimal  $T_{dep}$ , the estimated  $R_{dep}$ 's are  $2 \times 10^{-5} \text{ Å/s}$  and  $2 \times 10^{-8} \text{ Å/s}$ , respectively. It would take 3-3000 years to complete depositions at these rates on silicon, which is prohibitively slow. This remarkable decrease in the temperature to which films can be equilibrated and the dramatic increase in achievable thermodynamic stability can be attributed to the enhanced rate of SME, consistent with the direct observations of enhanced interfacial mobility and stability as discussed above.

# Reduced structural anisotropy

In PVD glasses, a preferred molecular orientation is adopted due to the equilibrium boundary conditions of the free surface, the degree of which depends on the depth at which the molecules are immobilized<sup>12</sup>. TPD molecules have in-plane orientation at the immediate free surface and out-of-plane orientation just below the first molecular layer<sup>8–11</sup>. As such, at low  $T_{dep}$  or fast  $R_{dep}$  where the mobile surface doesn't exist or is just one-molecular-layer thick, in-plane orientation is seen; if the mobile surface is roughly two-molecular-layers (intermediate deposition range), an out-of-plane orientation is adopted<sup>8,9,12</sup>; at higher  $T_{dep}$  and/or lower  $R_{dep}$  (close to  $T_g$ ), a thick enough surface layer is equilibrated, producing isotropic glasses.

On rigid substrates, a distinct molecular layering is also observed in GIWAXS experiments at intermediate  $T_{dep}$  (**Figure 2a**), which is stronger at lower  $R_{dep}$  (**Figure 2c**). Layering has been attributed either to the equilibrium surface structure<sup>25</sup> or out-of-equilibrium accelerated aging under a rigid glass structure below<sup>11,12</sup>. **Figure 2b-d** show that the layering peak has a much lower intensity on PDMS, and is insensitive to  $R_{dep}$  in the measured window. The weak layering is another indication that on PDMS the PVD glass is better equilibrated at larger depths away from the free surface.

To quantify the molecular orientation in GIWAXS experiments (Figures S18-S22), the Her-

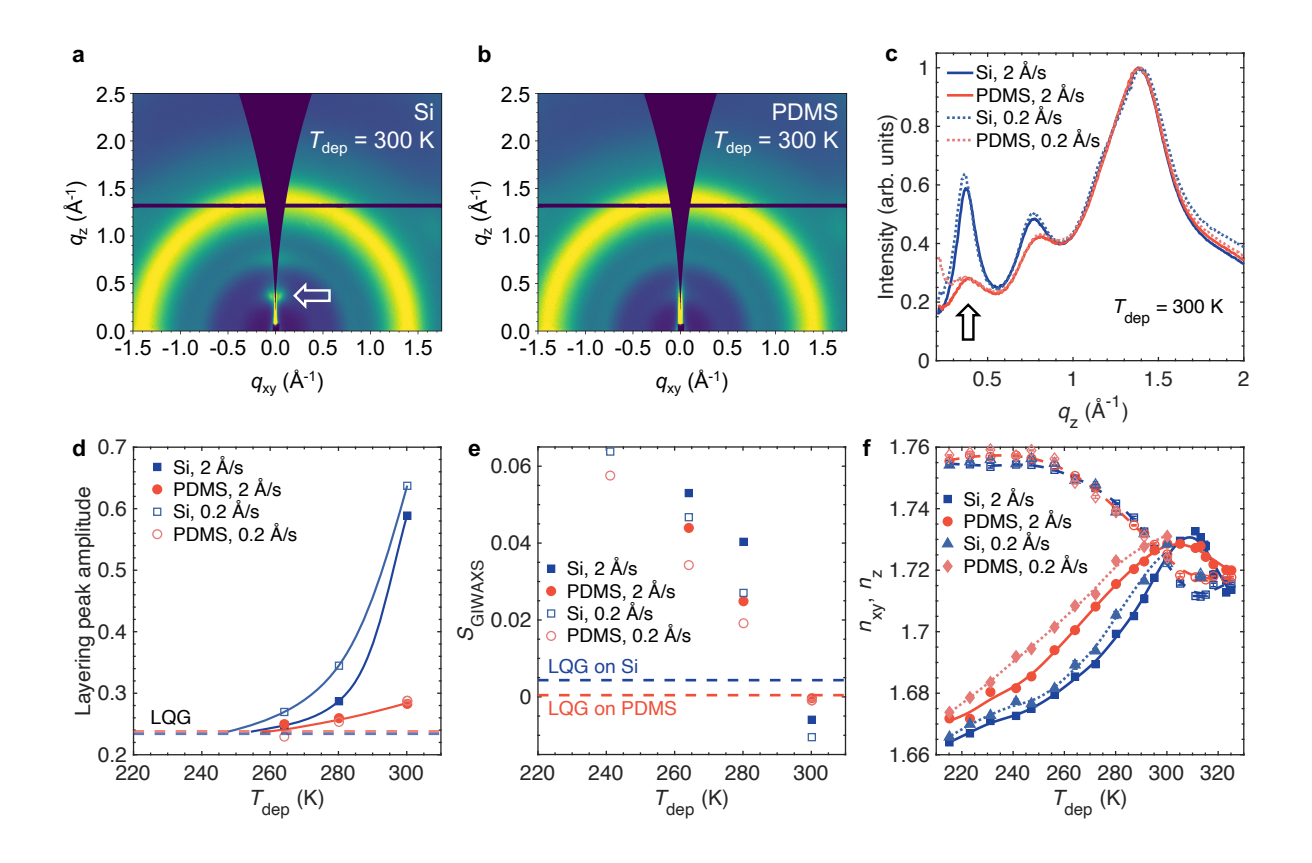


Figure 2. Structural anisotropy of TPD glasses deposited on 5 nm PDMS and silicon substrates. a,b, 2D GIWAXS patterns for films deposited on (a) silicon and (b) PDMS at  $T_{dep} = 300$  K,  $R_{dep} = 2$  Å/s. c, Normalized 1D GIWAXS profiles along the out-of-plane direction for films deposited at  $T_{dep} = 300$  K on silicon (blue) and PDMS (red) at  $R_{dep} = 2$  Å/s (solid lines) and  $R_{dep} = 0.2$  Å/s (dotted lines). The arrows in (a&c) denote an additional scattering feature along the out-of-plane direction at  $q_z \approx 0.4$  Å<sup>-1</sup>, corresponding to molecular layering. d, Normalized layering peak amplitude vs.  $T_{dep}$ . Colored lines are a guide to the eye. e, GIWAXS-derived orientation order parameter,  $S_{GIWAXS}$ , (calculated in the spectral range of 1.1 Å<sup>-1</sup>  $\leq q \leq 1.7$  Å<sup>-1</sup>) vs.  $T_{dep}$ . The dashed horizontal lines in (d&e) represent the corresponding values for LQGs. The error bars (standard error) are much smaller than the symbol size. f,  $n_{xy}$  (open symbols) and  $n_z$  (solid symbols) for films deposited on PDMS (red) and silicon (blue), measured by VASE at T = 298 K. Colored lines serve as guides for the eyes.

mans orientation order parameter<sup>46</sup> ( $S_{GIWAXS}$ ) was calculated for the primary diffraction peak at  $q \approx 1.4 \text{ Å}^{-1}$  (**Figure 2e**). Consistent with previous reports<sup>8,22</sup>, SGs deposited on silicon have preferred in-plane orientation at  $T_{dep} \leq 280 \text{ K}$  ( $S_{GIWAXS} > 0$ ), and slight out-of-plane orientation ( $S_{GIWAXS} < 0$ ) at  $T_{dep} = 300 \text{ K}$ . Deposition at a slower rate (0.2 Å/s) reduces the orientational

anisotropy (smaller absolute value of  $S_{GIWAXS}$ ), as the glass has more time to equilibrate. On PDMS, SGs are more isotropic than those on silicon at all deposition conditions (**Figure 2e**), which is also corroborated by measurements of optical birefringence; the difference between out-of-plane  $(n_z)$  and in-plane  $(n_{xy})$  refractive indices (**Figures 2f&S23**). For  $T_{dep} \leq 300$  K, while  $n_{xy}$  is similar on PDMS and silicon,  $n_z$  is remarkably larger. The increases in  $n_z$  upon changing the substrate from silicon to 5 nm PDMS (up to 0.02, **Figure 2f**) and 13 nm PDMS (up to 0.03, **Figure S23**) are much larger than that upon reducing  $R_{dep}$  by one decade on silicon ( $\approx 0.006$ ). In contrast, at  $T_{dep} > 300$  K, larger  $n_{xy}$  values are measured on PDMS compared to silicon, indicating reduced out-of-plane orientation (smaller  $n_z - n_{xy}$ ). In all cases density, measured through  $\langle n \rangle = \sqrt{(2n_{xy}^2 + n_z^2)/3}$ , is increased on PDMS (**Figures 1e&S17**).

Overall, the data in **Figure 2** indicates that glasses deposited on PDMS have an accelerated rate of SME over a thicker layer, providing a more efficient pathway to equilibrate the structure that can be achieved by reducing  $R_{dep}$  by more than 7 decades. As seen in **Figures 2e,f&S23**, even at low temperatures,  $T_{dep} < 280$  K, where the roughness and  $\delta \langle n \rangle$  become too small to directly visualize the thickness of mobile surface layer, glasses on PDMS are more isotropic ( $n_z$  is larger,  $S_{GIWAXS}$  is smaller), meaning that the rate of SME is enhanced on PDMS compared to silicon, in the entire  $T_{dep}$  range available in this study.

The LQG is also more isotropic and has a higher average density on PDMS. The small orientational anisotropy on silicon ( $S_{GIWAXS}(LQG) = 0.0043$ , **Figure 2e**) is attributed to the stress due to the mismatched glass/substrate expansion coefficients<sup>22,47</sup>. On PDMS, the internal stresses are reduced producing isotropic glasses ( $S_{GIWAXS}(LQG) = 0.0004$ ). These stress-induced effects are not expected to affect the SCL state. Surprisingly, even in the SCL, the refractive index is higher on PDMS than on silicon by  $\approx 0.0013$  (**Figure S24**), indicating a denser SCL. Previous measurements on TPD<sup>41</sup> and polystyrene<sup>48</sup> have shown higher density in ultra-thin glass and SCL films, which in TPD was attributed to the existence of a previously unknown low-temperature, high-density phase<sup>41</sup>. Here, it appears that elements of these structures persist to longer length scales on PDMS (180 nm thick films).

# Length scale of the substrate influence on glass structure

The effect of the PDMS substrate on enhancing the rate of SME and generating more isotropic structures fades as the film thickness is increased. For example, as seen in **Figure 3** (2D patterns in **Figure S25**), the layering peak amplitude increases with deposited film thickness on PDMS,

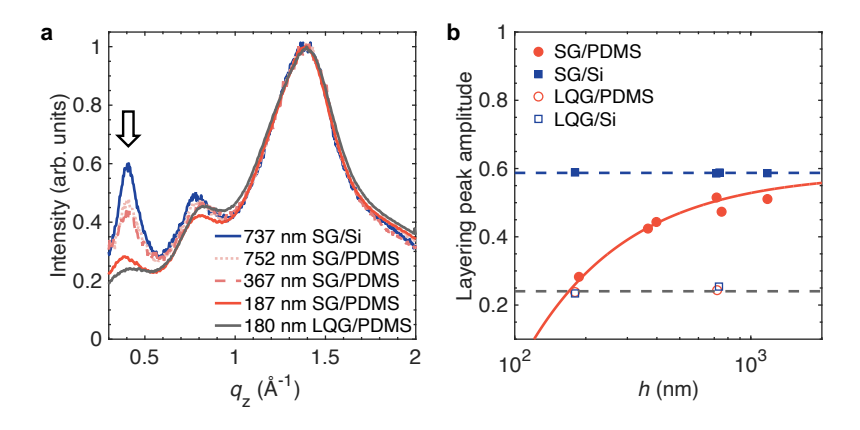


Figure 3. Layering peak amplitude of TPD glasses as a function of film thickness. a, Normalized 1D GIWAXS profiles along the out-of-plane direction ( $q_z$ ) for films of different thicknesses deposited on 5 nm PDMS and silicon ( $T_{dep} = 300 \text{ K}$ ,  $R_{dep} = 2 \text{ Å/s}$ ), and an LQG film on PDMS. The arrow denotes the layering peak position ( $q_z \approx 0.4 \text{ Å}^{-1}$ ). b, Normalized layering peak amplitude vs. film thickness. Filled symbols represent PVD films and open symbols are LQGs films on PDMS (red circle) and silicon (blue squares). The dashed lines show the averaged values for PVD films on silicon (blue,  $I_{Si} = 0.587$ ), and LQGs films on both PDMS and silicon (gray,  $I_{LQG} = 0.240$ ), respectively. The solid red line represents the fit of a two-layer model, with a length scale of  $\delta = 170 \pm 9 \text{ nm}$ , as detailed in the text.

asymptotically approaching the corresponding value on silicon, which is independent of film thickness (**Figure 3b**). For a  $\sim$ 180 nm thick TPD film deposited on PDMS, the layering peak amplitude is close to the value measured in LQG films (lower bound value). The data in **Figure 3b** fits well to a two-layer model (solid curve), assuming that the region near the PDMS substrate has the same intensity as the LQG (no layering) while the remaining film exhibits layered packing similar to those of films deposited on silicon (details in **Methods**). The thickness of this interfacial region is determined to be  $\delta = 170\pm9$  nm, showing the substantial range over which the glass structure remains isotropic due to the influence of the PMDS substrate.

# Controlling the structure and stability through substrate modulus

To further study the effect of substrate modulus, 5 nm PDMS layers were prepared at various curing temperatures ( $T_{curing}$ ) from 295 K to 433 K, with Young's moduli between  $\sim$ 3.9 MPa to  $\sim$ 5.3 MPa, estimated based on AFM indentation measurements and the bulk dependence of the modulus on curing temperature<sup>49</sup> (**Supplementary Note 1**). The data was also compared

to results on a 13 nm thick PDMS substrate, which is less affected by silicon and has lower E ( $E=2.8\pm0.2$  MPa, cured at 383 K for 1 h). **Figure 4** shows a strong correlation between the TPD film properties and the PDMS modulus (E-dependence of other variables in **Figure S26**). **Figure 4a** shows that decreasing the PDMS modulus increases the TPD surface roughness (i.e. the mobile surface thickness, AFM images in **Figures S7&S27**), allowing the deposited molecules to equilibrate to higher relative density (**Figure 4b**) and more isotropic (smaller  $n_{xy} - n_z$ , **Figure 4c**) states. Remarkably, decreasing the PDMS modulus from  $\approx 5.3$  MPa to  $\approx 2.8$  MPa results in an increase in  $\Delta \rho$  from  $\approx 2\%$  to  $\approx 2.5\%$  for as-deposited samples. Upon pre-heating, more stable interfacial regions are transformed (larger  $\delta \langle n \rangle$  at lower E, **Figure S26**), leading to a larger decrease in the average film density (**Figure 4b**). However, even after pre-heating a dependence on E still persists, with reducing E by 2.5 MPa is equivalent to reducing  $R_{dep}$  by at least  $10^3$  times on silicon. These effects are also observed at lower  $T_{dep}$ 's (**Figures S17&S23**).

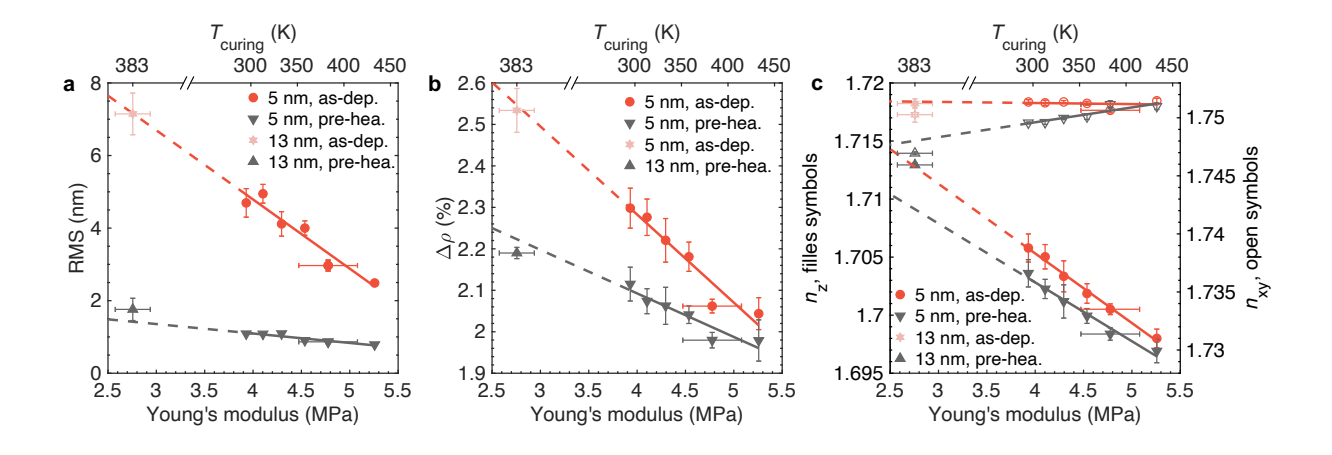


Figure 4. Effect of PDMS modulus on the structure and stability of TPD SGs. a, Surface roughness, **b**,  $\Delta \rho$ , and **c**,  $n_z$  (filled symbols) and  $n_{xy}$  (open symbols) of as-deposited (red) and pre-heated (gray) TPD films vs. the estimated Young's modulus (bottom axis) and  $T_{curing}$  (top axis) of the PDMS films. Films were deposited at  $T_{dep} = 264$  K and  $R_{dep} = 2$  Å/s. The solid lines are linear fits to the data on 5 nm PDMS substrates (red circles and downward-pointing triangles), which are extrapolated to the values as shown by the dashed lines. The data on 13 nm PDMS substrate (cured at 383 K for 1 h) are shown as light red hexagrams and upward-pointing triangles. The error bars represent standard error.

It is important to emphasize that  $\Delta \rho \simeq 2\%$  achieved on the stiffest PDMS film ( $E \approx 5.3$  MPa, cured at 433 K), is not experimentally accessible on silicon, as it would take  $\sim 4$  months of deposition even at the optimal  $T_{dep}$ . Furthermore, it is important to investigate the feasibility of

transferring these glasses onto alternative support substrates without compromising their properties, which should be a subject of future studies.

### **Outlook**

In summary, we demonstrate that surface-mediated SG formation is dramatically accelerated when PVD is performed on soft low-modulus substrates such as PDMS. The vapor-deposited glass density and structure can be precisely controlled over a broad and previously inaccessible range, by varying the the modulus of an ultrathin rubber layer, resulting in glasses with  $\sim 2.5\%$  larger density than LQGs. To make such high-density SGs, it would take thousands of years of slow deposition on silicon or millions of years of LQG aging. This is because, the free surface mobility is dynamically influenced by the soft substrate interface at distances of  $\sim 170$  nm away, resulting in thicker and more mobile surface layers. This discovery represents a paradigm-shifting approach to manipulating the properties of SGs through the selection of an appropriate substrate, which can be of interest in applications such as organic semiconductors where controlling other deposition parameters is challenging and costly.

The enhanced mobility afforded by the soft substrate can also open new opportunities to equilibrate bulk glasses at lower temperatures, creating a unique window for exploring low-temperature glass phases in their bulk state. The decoupling of the surface and bulk dynamics (**Figures 1d&S12**), the higher density of the interfacial layers that could exceed the extrapolated bulk density (**Figure S17**) and the higher density of the SCL on PDMS compared to silicon (**Figure S24**) all point to anomalous behavior that may be related to low-temperature phases previously observed only in thin TPD films<sup>41</sup>. The surprisingly large length scales of coupled dynamics between the free surface and the soft substrate indicate the critical role of elasticity in glass transition<sup>50</sup>, which merit more experimental and theoretical explorations, as the underlying origins of these effects are currently unknown.

# **METHODS**

# Sample preparation

**PDMS** substrate preparation. Thin film PDMS substrates were made from Sylgard 184 silicone elastomer kit (Dow Corning). The base and curing agents with a mass ratio of 10:1 were mixed and dissolved in toluene to prepare a stock solution of 10wt.% PDMS, which was shaken and ultrasonicated for 10 min for better dissolution and mixing. Diluted PDMS solutions with concentrations of 0.2wt.% and 0.5wt.% were prepared from the stock solution and spun-cast on silicon wafers (<100>-oriented, Virginia Semiconductor Inc.) at a rotating speed of 5000 rpm. PDMS films with  $5\pm1$  nm and  $13\pm1$  nm thicknesses (as measured by SE) were prepared from the 0.2wt.% and 0.5wt.% dilute solutions, respectively. The spun-cast PDMS films were typically cured under vacuum at 383 K for 1 h, which also removed the residual solvent. For data shown in Figure 4, curing of PDMS was performed at 313 K, 333 K, 358 K, 383 K, 433 K, respectively, for 1 h, and at room temperature (295 $\pm$ 1 K) for 51 $\pm$ 7 h. The surface morphology and roughness of PDMS films were characterized on various samples, by AFM at various temperatures ranging from 300 K to 353 K, the highest temperature used in transformation experiments. These measurements were repeated at the same temperatures upon cooling, after a 20 min isothermal hold at 353 K. As shown in Figure S3, the RMS roughness at all temperatures was < 1 nm and similar to the inherent roughness of the silicon substrate (Figure S2). Additional control experiments were performed to explore the potential role of uncrosslinked monomers and other free small molecules, and no difference was observed in PVD film properties before and after the removal soaking of PDMS films in toluene. More details are included in **Supplementary Note 3** and **Figures S28&S29**.

**TPD film preparation.** TPD was purchased from Sigma-Aldrich (purity >99%), and used without further purification. Vapor-deposition of TPD was carried out in a custom-designed ultra-high vacuum (UHV) chamber, with a base pressure of  $\sim 10^{-7}$  Torr, as described in our previous publication<sup>51</sup>. The distance between the deposition source and the temperature-controlled substrates was approximately 25 cm. TPD glasses were deposited at two deposition rates of  $R_{dep} = 2\pm0.2$  Å/s and  $0.2\pm0.03$  Å/s, which were monitored using a quartz crystal microbalance (QCM, Inficon STM-2 USB thin film rate/thickness monitor) placed near the substrate stage. A shutter between the TPD source and the substrate was opened to start deposition after  $R_{dep}$  stabilized at the target value and closed once the target thickness was reached. The UHV chamber is equipped with three independently temperature-controlled sample stages, each holding 6 substrates with

a size of 1.5 cm  $\times$  1.5 cm. All three stages were utilized during each deposition, each holding 3 substrates of the same type, PDMS and silicon. This approach was used to reduce errors due to variations in deposition conditions. At least three independent depositions were performed at each  $T_{dep}$  and  $R_{dep}$ . TPD films deposited on 13 nm thick PDMS substrates readily fractured in the course of thermal transformation. Therefore, most of the data presented here were based on depositions performed on the 5 nm thick PDMS substrates.

### **AFM** characterization

The surface morphology of various substrates and PVD glass films, deposited under various conditions, was measured using a Bruker Dimension Icon AFM. AFM images were collected in tapping mode with an image resolution of 512 pixels × 512 pixels, using probes from Budget Sensors (Tap300Al-G, 10 nm tip radius of curvature). The RMS roughness and the radial power spectral density function (PSDF) of the surface morphology were calculated using the Gwyddion software.

AFM indentation measurements were performed on 5 nm and 13 nm PDMS films, as well as a bulk PDMS film (~0.5 mm thick) with similar standard curing conditions, to measure their moduli (**Figure S1a**). For analyzing the data of bulk film, Johnson-Kendall-Roberts (JKR) contact mechanics model<sup>52</sup> was used, and for the ultrathin films, indentation results were analyzed with a thin film model proposed by Reedy<sup>53</sup>. To estimate the Young's moduli for thin films cured at different temperatures, it was assumed that the slope of curing temperature dependence of Young's modulus in these films was the same as that of bulk PDMS<sup>49</sup> and the data was accordingly shifted (**Figure S1b**). More details can be found in **Supplementary Note 1**.

### SE characterization

SE measurements. SE measurements were performed on a J. A. Woollam M-2000V ellipsometer equipped with a Linkam stage (THMS600) for temperature control. A thin layer of high-temperature vacuum grease (Apiezon PFPE 501) was applied to ensure good thermal contact between the substrate and the stage. The ellipsometric angles  $\Psi$  (amplitude change) and  $\Delta$  (phase change) were collected in the spectral wavelength range of 370 nm>  $\lambda$  >1700 nm. To improve accuracy, zone-averaged measurements at constant temperature were performed using VASE at various incident angles from 55° to 75° at every 5°, with an acquisition time 20 s each. In zone-averaged measurements, the SE data was averaged based on two measurements acquired with the polarizer rotated by 90°, which can eliminate systematic measurement errors. For *in* 

situ dilatometry or isothermal experiments, the incident angle was fixed at 70°, and the data were collected with zone averaging at 2 s to 50 s intervals depending on the duration of the experiment.

When modeling the SE data using the CompleteEase software, the optical properties of the deposited films on PDMS were modeled using a 4-layer model, including from bottom to top a silicon layer, a 1.0 nm thick native silicon oxide layer with known parameters, a transparent Cauchy layer corresponding to the PDMS layer, and another anisotropic Cauchy layer corresponding to the TPD glass. The refractive index of the birefringent transparent Cauchy layers can be described as:

$$n_{xy} = A_{xy} + \frac{B}{\lambda^2},\tag{1}$$

$$n_z = A_z + \frac{B}{\lambda^2},\tag{2}$$

where  $n_{xy}$  and  $n_z$  are the in-plane and out-of-plane refractive indices, respectively, and  $A_{xy}$ ,  $A_z$ , and B are the Cauchy fit parameters. In this model, the imaginary part of the refractive index is assumed to be zero. In the isotropic model,  $A_{xy} = A_z$ .

VASE measurements were performed for the PDMS substrates prior to the deposition of TPD, and the fitted parameters were used as known parameters when modeling the ellipsometry data. The ellipsometry data for the silicon substrate are available in the CompleteEASE library, therefore, only the parameters for the TPD layer were fitted. Supplementary control experiments and analyses were conducted, which affirm the robustness and reliability of the 4-layer model, as detailed in **Supplementary Note 4** and **Figures S30&S31**.

The film thickness (h) was also used as an independent fit parameter. To avoid the strong absorbance of TPD at  $\lambda < 400$  nm (ref.<sup>41</sup>), the SE data were fitted in the wavelength range of 550 nm  $< \lambda < 1700$  nm. The refractive indices reported here are all calculated at  $\lambda = 632.8$  nm.

To obtain the temperature-dependent values of the refractive indices of the PDMS substrates, the  $\sim$ 13 nm thick PDMS films were characterized by VASE measurements at various isothermal temperatures from 298 K to 393 K at every 5 K both upon heating and cooling. The VASE data were fitted in the wavelength range of 370 nm  $> \lambda > 1700$  nm. **Figure S32** shows the isotropic Cauchy parameters A, B, and thickness h as a function of temperature for PDMS substrates. The heating and cooling data between 298 K and 363 K were fitted globally to a linear function, which

gave:

$$A_{PDMS} = 1.4767 - 1.8967 \times 10^{-4} T, (3)$$

$$B_{PDMS} = 5.7808 \times 10^{-3} - 1.2974 \times 10^{-5} T, \tag{4}$$

$$h_{PDMS}(nm) = 10.2658 + 8.5802 \times 10^{-3}T.$$
 (5)

The  $T_g$  of PDMS is  $\approx 148$  K (ref.<sup>54</sup>). At 298 K < T < 363 K, the linear coefficient of thermal expansion (CTE) for the PDMS film was measured  $(6.69 \pm 0.19) \times 10^{-4}$  K<sup>-1</sup>. When a film is supported on a rigid substrate, the in-plane of the film is constrained to match that of the substrate. Therefore, the experimentally measured CTE from the temperature dependence of the PDMS film thickness,  $\alpha_{measured}$ , is different from that of the stress-free, bulk samples, but is altered by the CTE of the substrate,  $\alpha_{Si}$ , and the Poisson's ratio of PDMS,  $\nu_{PDMS}$ . Pye and Roth<sup>55</sup> have derived the equation that can be used to determine the "true" (or corrected) value of CTE from the film thickness measurements of PDMS:

$$\alpha_{PDMS} = \frac{1 - \nu_{PDMS}}{1 + \nu_{PDMS}} \alpha_{measured} + \frac{2\nu_{PDMS}}{1 + \nu_{PDMS}} \alpha_{Si}. \tag{6}$$

Using  $\alpha_{measured} = 6.69 \times 10^{-4} \text{ K}^{-1}$ ,  $v_{PDMS} = 0.48$  (ref.<sup>56</sup>), and  $\alpha_{Si} = 3 \times 10^{-6} \text{ K}^{-1}$  (ref.<sup>55</sup>), we get  $\alpha_{PDMS} = 2.37 \times 10^{-4} \text{ K}^{-1}$ . This value is smaller than the reported value for bulk samples in the technical data sheet by Dow<sup>57</sup> (3.40 × 10<sup>-4</sup> K<sup>-1</sup>), suggesting that the silicon substrate suppresses the thermal expansion of the ~13 nm thick PDMS film. At 298 K, the measured refractive index for PDMS is about 1.425±0.002, in agreement with the value of 1.4225 as reported in the technical data sheet<sup>57</sup> as well as other literature reports<sup>58–60</sup>.

For the  $\sim$ 5 nm PDMS films, VASE measurements were performed only at 298 K, and the data were fitted by isotropic Cauchy models using the same A and B values from the thicker films, leaving only h as the fitting parameter. When fitting the SE data of *in situ* transformation and isothermal annealing, the temperature dependence of A and B as shown in **Equations 3,4** are used for both the thicker and the thinner PDMS substrates, and the temperature dependence of h was derived from **Equation 5** assuming that the value of CTE is the same for films of different thicknesses. At least 50% of each batch of spun-coated substrates were characterized with VASE at 298 K.

Calculation of relative density based on refractive index. For optically anisotropic films  $(n_{xy} \neq n_z)$ , the average refractive index  $(\langle n \rangle)$  was calculated as:

$$\langle n \rangle = \sqrt{\frac{n_x^2 + n_y^2 + n_z^2}{3}} = \sqrt{\frac{2n_{xy}^2 + n_z^2}{3}}.$$
 (7)

The density of glass is correlated with its transparent refractive index through the Lorentz-Lorenz equation<sup>45</sup>,

$$\frac{n^2 - 1}{n^2 + 2} = \frac{\alpha N_A \rho}{3\varepsilon_0 M_W},\tag{8}$$

where  $\rho$  is density,  $\alpha$  is the molecular polarizability,  $N_A$  is the Avogadro number,  $\varepsilon_0$  is the permittivity of the free space, and  $M_W$  is the molecular molar mass. This equation indicates that n can be used as an independent measure of density without relying on thickness change upon film transformation. Our previous work<sup>41</sup> has demonstrated that this correlation holds for TPD glass films over a broad range of film thicknesses.

Assuming the changes in n and  $\rho$  are small, we have:

$$\frac{6n}{(n^2+2)^2}dn = \frac{\alpha N_A}{3\varepsilon_0 M_W}d\rho. \tag{9}$$

By dividing **Equation 9** by **Equation 8** we get the relative changes:

$$\frac{d\rho}{\rho} = \frac{6n^2}{(n^2 + 2)(n^2 - 1)} \frac{dn}{n}.$$
 (10)

We define  $\Delta \rho = (\rho - \rho_{LQG})/\rho$ , and  $\Delta n = (n - n_{LQG})/n$ , to substitute for  $d\rho/\rho$  and dn/n respectively, we have:

$$\Delta \rho = \frac{6n^2}{(n^2 + 2)(n^2 - 1)} \Delta n. \tag{11}$$

With Equation 11 the relative density change  $(\Delta \rho)$  can be calculated using the relative change in the refractive index  $(\Delta n)$ , compared to the values of LQG at 298 K. For birefringent samples,  $\langle n \rangle$  is used instead of n.

# Pre-heating procedure to reduce roughness and measure $\delta\langle n \rangle$

Compared to the glasses deposited on silicon (**Figure S4**), those deposited on PDMS show surface patterns with large roughness values that are increasingly more pronounced at higher  $T_{dep}$  values or at slower  $R_{dep}$  (**Figures S5-S7**). To calculate the lateral correlation length ( $L_{corr}$ ) of the surface patterns, the PSDF was obtained by calculating the two-dimensional Fourier transform of each AFM image. The radial PSDF vs. radius ( $W_r$ ) was then calculated by integrating along the symmetric angular direction.  $L_{corr}$  was measured as  $L_{corr} = 2\pi/k_{max}$ , where  $k_{max}$  is the spatial frequency at which  $W_r$  has a maximum. From **Figure S8** we can see that  $L_{corr}$  of these patterns on the glasses deposited on PDMS increases with increasing  $T_{dep}$  and decreasing  $R_{dep}$  as indicated by the left shift of the PSDF peak.

Such a structured surface morphology with lateral length-scales (Figure S8c) comparable with the wavelengths of SE measurements can potentially lead to interference of the reflected light when the roughness is large, and thus affect the fitting of the SE data. However, the surface roughness decreases rapidly when as-deposited samples are pre-heated to 335 K, without affecting the properties of the bulk film as transformation occurs only at the interfaces and propagates towards bulk at an extremely slow velocity ( $\sim 10^{-3}$  nm/s, ref.<sup>42</sup>). As shown in **Figure S11**, this pre-heating procedure does not systematically affect the mean-square error (MSE) of the SE fitting, but results in the transformation of the interfacial regions of the glass, with reduced  $T_g$  and thermal stability, thus leading to the reduction of the surface roughness and its flattening (detailed discussions in the main text). Therefore, to reduce the effect of interfacial regions which have higher refractive indices and measure the bulk glass stability, samples deposited on PDMS with large initial RMS roughness and  $\delta\langle n \rangle$ ;  $T_{dep} \geq 280$  K for  $R_{dep} = 2$  Å/s and  $T_{dep} \geq 264$  K for  $R_{dep} = 0.2$  Å/s, were pre-heated before bulk transformation experiments. Two procedures of pre-heating were performed, heating the samples to 335 K and immediately cooling back to room temperature at a heating/cooling rate of 10 K/min, or heating at 60 K/min to temperatures such as 325 K and holding at this temperature until the interfacial regions were fully transformed as indicated by plateauing of the refractive indices, monitored by in situ SE measurements, then cooling back to room temperature at 10 K/min. Neither procedure resulted in bulk transformation of these samples. After pre-heating, the surface morphology is remarkably flattened due to the transformation of the surface region (Figures S5-**S7**). VASE measurements at 298 K were performed before and after pre-heating to measure  $\delta \langle n \rangle$ , the degree of transformation of the interfacial regions.

As the thickness of the mobile interfacial regions and therefore stable interfacial regions are reduced at lower temperatures, glasses deposited at lower  $T_{dep}$  have smaller surface roughness, and pre-heating does not induce obvious changes in the refractive indices (**Figures S9&S10**). As an additional verification, TPD films deposited on silicon were pre-heated at various  $T_{dep}$ 's. No change was observed in  $n_{xy}$  and  $n_z$  of these films even with prolonged heating times (**Figure S14**), indicating that the thickness of the mobile interfacial regions is small on silicon substrate and such pre-heating procedures transform only the interfacial regions without affecting the properties of the bulk film.

Upon pre-heating, the interfacial regions are expected to have a lower density (LQG density) than the bulk of the film. In addition, it is possible that these films have a gradient of density close to each interface. However, given that an independent measurement of these values is not feasible

in the measured data, to avoid overfitting in SE modeling, a uniform layer was used for the TPD glass, which assumes uniform properties for both the bulk and the interfacial regions. As a result, the refractive index and density of the bulk TPD glass should be higher than those obtained from the pre-heated samples (**Figure S17**). Therefore, the results shown in **Figure 1f** serve as lower limits of the relative density for glasses deposited on PDMS.

### **GIWAXS** characterization

**GIWAXS** measurements. GIWAXS measurements for  $\sim$ 180 nm thick TPD films were carried out at 12-ID (Soft Matter Interfaces) beamline at the National Synchrotron Light Source II (NSLS-II) of the Brookhaven National Laboratory (BNL). A Pilatus 900k-W detector with a sample-to-detector distance of 277 mm was used. The incident angle was set to be 0.1°. The energy of the X-ray beam was set to 16.1 keV ( $\lambda$  = 0.77009 Å). The X-ray scattering experiments were performed under a vacuum of less than  $6\times10^{-3}$  Torr. To cover a broad range of scattering angles, 4 images were collected with the detector being moved horizontally on a fixed arc to 4 different positions: 0°, 2°, 18°, and 20° relative to the incident beam. Each image was collected with an exposure time of 0.3 s. No discernible change was found for longer exposure times of 0.5 s and 1 s, indicating that the samples could withstand X-ray beam radiation during these exposure periods. A Python-based package<sup>61</sup> developed at the NSLS-II was used to perform post-acquisition data processing.

Additional GIWAXS experiments were conducted for thick TPD films (>360 nm) vapor-deposited on silicon and PDMS substrates at  $T_{dep} = 300$  K and  $R_{dep} = 2$  Å/s, using a Xeuss 2.0 X-ray scattering instrument (Xenocs, at LRSM UPenn). The X-ray was generated by a Cu  $K_{\alpha}$  source with a beam energy of 8.04 keV ( $\lambda = 1.54189$  Å). The X-ray scattering experiments were performed under a vacuum of less than  $1 \times 10^{-2}$  Torr. The incident angle was set to 0.2°. The detector (Pilatus 1M) was placed at a distance of  $\approx$ 180 mm behind the sample. The sample-to-detector distance was calibrated using silver behenate, a standard reference material. TPD glass is not a strong X-ray scatterer and the beam flux of the in-house X-ray source is orders of magnitude lower than that of the synchrotron beam. As such, to obtain better data quality, the scattering pattern was recorded for 150 min and 360 min, for samples with thickness >700 nm and 360 – 400 nm, respectively. The data processing was performed using the Foxtrot software developed by Synchrotron SOLEIL, France.

Azimuthal integration from the 2D scattering patterns was performed to obtain the 1D scatter-

ing profiles along the in-plane  $(q_{xy})$  and out-of-plane  $(q_z)$  directions. The azimuthal angle  $(\psi)$  was defined as:  $\psi = 0^{\circ}$  along the  $q_z > 0$  axis,  $\psi = -90^{\circ}$  along the  $q_{xy} < 0$  axis, and  $\psi = 90^{\circ}$  along the  $q_{xy} > 0$  axis. Azimuthal integration between  $0^{\circ} \le \psi \le 15^{\circ}$  was performed to obtain the 1D scattering profiles along  $q_z$ , and between  $75^{\circ} \le \psi \le 90^{\circ}$  to obtain the 1D scattering profiles along  $q_{xy}$ , respectively. Azimuthal integration between  $0^{\circ} \le \psi \le 90^{\circ}$  provides the total scattering intensity. Calculation of the orientational order parameter. The GIWAXS-derived orientational order parameter  $S_{GIWAXS}$  can be defined as:

$$S_{GIWAXS} = \frac{1}{2} (3\langle \cos^2 \psi \rangle - 1). \tag{12}$$

 $S_{GIWAXS}$  was calculated for the data collected at NSLS-II, using a Python-based package. The  $\langle cos^2 \psi \rangle$  was calculated based on the average of the scattering intensity  $I(\psi)$  in the spectral range of  $1.1 \le q \le 1.7 \text{ Å}^{-1}$  along  $0^\circ \le \psi \le 90^\circ$ , and was defined as:

$$\langle \cos^2 \psi \rangle = \frac{\int_0^{90} I(\psi) \cdot \cos^2 \psi \cdot \sin \psi \, d\psi}{\int_0^{90} I(\psi) \cdot \sin \psi \, d\psi}.$$
 (13)

The limiting values of  $S_{GIWAXS}$  are +1.0 and -0.5, where  $S_{GIWAXS}$  = +1.0 means the scattering is predominantly in the out-of-plane (along  $q_z$ ) direction and the molecules are oriented parallel to the substrate, while  $S_{GIWAXS}$  = -0.5 indicates predominantly in-plane scattering (along  $q_{xy}$ ) corresponding to molecular orientations normal to the substrate. An  $S_{GIWAXS}$  = 0 corresponds to isotropic molecular orientation.  $S_{GIWAXS}$  calculations were performed on three samples independently deposited at  $T_{dep}$  = 300 K and  $R_{dep}$  = 0.2 Å/s on PDMS substrates, measured at the NSLS-II. The error bar for  $S_{GIWAXS}$  is much smaller than the symbol size for the data shown in **Figure 2e**.

**Two-layer model to obtain the length scale of the substrate influence on layering.** The data in **Figure 3b** fits well to a two-layer model, assuming that the region near the PDMS substrate has the same intensity as the LQG (no layering) while the remaining film exhibits layered packing similar to those of films deposited on silicon:

$$I_{PDMS}(h) = I_{LQG} + (I_{Si} - I_{LQG}) \times (1 - \frac{\delta}{h}), \tag{14}$$

where  $I_{PDMS}$ ,  $I_{LQG}$ , and  $I_{Si}$  are the normalized layering peak amplitudes for a film with thickness h deposited on PDMS, the lower bound measured in LQG ( $I_{LQG} = 0.240$ ), and the upper bound measured in films deposited on silicon ( $I_{LQG} = 0.587$ ), respectively. Here,  $\delta$  is the thickness of the layer without layering peak ( $I_{PDMS}(\delta) = I_{LQG}$ ), and is the only fit parameter.

# REFERENCES

- <sup>1</sup>Z. Fakhraai and J. Forrest, "Measuring the surface dynamics of glassy polymers," Science **319**, 600–604 (2008).
- <sup>2</sup>Z. Yang, Y. Fujii, F. K. Lee, C.-H. Lam, and O. K. Tsui, "Glass transition dynamics and surface layer mobility in unentangled polystyrene films," Science **328**, 1676–1679 (2010).
- <sup>3</sup>Y. Chai, T. Salez, J. D. McGraw, M. Benzaquen, K. Dalnoki-Veress, E. Raphaël, and J. A. Forrest, "A direct quantitative measure of surface mobility in a glassy polymer," Science **343**, 994–999 (2014).
- <sup>4</sup>L. Zhu, C. Brian, S. Swallen, P. Straus, M. Ediger, and L. Yu, "Surface self-diffusion of an organic glass," Physical Review Letters **106**, 256103 (2011).
- <sup>5</sup>Y. Zhang and Z. Fakhraai, "Decoupling of surface diffusion and relaxation dynamics of molecular glasses," Proceedings of the National Academy of Sciences **114**, 4915–4919 (2017).
- <sup>6</sup>Z. Hao, A. Ghanekarade, N. Zhu, K. Randazzo, D. Kawaguchi, K. Tanaka, X. Wang, D. S. Simmons, R. D. Priestley, and B. Zuo, "Mobility gradients yield rubbery surfaces on top of polymer glasses," Nature **596**, 372–376 (2021).
- <sup>7</sup>S. F. Swallen, K. L. Kearns, M. K. Mapes, Y. S. Kim, R. J. McMahon, M. D. Ediger, T. Wu, L. Yu, and S. Satija, "Organic glasses with exceptional thermodynamic and kinetic stability," Science **315**, 353–356 (2007).
- <sup>8</sup>S. S. Dalal, D. M. Walters, I. Lyubimov, J. J. de Pablo, and M. Ediger, "Tunable molecular orientation and elevated thermal stability of vapor-deposited organic semiconductors," Proceedings of the National Academy of Sciences **112**, 4227–4232 (2015).
- <sup>9</sup>I. Lyubimov, L. Antony, D. M. Walters, D. Rodney, M. Ediger, and J. J. de Pablo, "Orientational anisotropy in simulated vapor-deposited molecular glasses," The Journal of chemical physics **143**, 094502 (2015).
- <sup>10</sup>A. R. Moore, G. Huang, S. Wolf, P. J. Walsh, Z. Fakhraai, and R. A. Riggleman, "Effects of microstructure formation on the stability of vapor-deposited glasses," Proceedings of the National Academy of Sciences 116, 5937–5942 (2019).
- <sup>11</sup>A. Zhang, A. R. Moore, H. Zhao, S. Govind, S. E. Wolf, Y. Jin, P. J. Walsh, R. A. Riggleman, and Z. Fakhraai, "The role of intramolecular relaxations on the structure and stability of vapor-deposited glasses," The Journal of chemical physics 156, 244703 (2022).
- $^{12}$ P. Luo and Z. Fakhraai, "Surface-mediated formation of stable glasses," Annual Review of Phys-

- ical Chemistry 74, 361-389 (2023).
- <sup>13</sup>K. L. Kearns, T. Still, G. Fytas, and M. Ediger, "High-modulus organic glasses prepared by physical vapor deposition," Advanced Materials **22**, 39–42 (2010).
- <sup>14</sup>S. S. Dalal, Z. Fakhraai, and M. D. Ediger, "High-throughput ellipsometric characterization of vapor-deposited indomethacin glasses," The Journal of Physical Chemistry B **117**, 15415–15425 (2013).
- <sup>15</sup>P. Luo, C. Cao, F. Zhu, Y. Lv, Y. Liu, P. Wen, H. Bai, G. Vaughan, M. Di Michiel, B. Ruta, and W.-H. Wang, "Ultrastable metallic glasses formed on cold substrates," Nature communications 9, 1–7 (2018).
- <sup>16</sup>P. Luo, F. Zhu, Y.-M. Lv, Z. Lu, L.-Q. Shen, R. Zhao, Y.-T. Sun, G. B. Vaughan, M. Di Michiel, B. Ruta, and W.-H. Wang, "Microscopic structural evolution during ultrastable metallic glass formation," ACS Applied Materials & Interfaces 13, 40098–40105 (2021).
- <sup>17</sup>J. Ràfols-Ribé, P.-A. Will, C. Hänisch, M. Gonzalez-Silveira, S. Lenk, J. Rodríguez-Viejo, and S. Reineke, "High-performance organic light-emitting diodes comprising ultrastable glass layers," Science advances **4**, eaar8332 (2018).
- <sup>18</sup>S. E. Wolf, S. Fulco, A. Zhang, H. Zhao, P. J. Walsh, K. T. Turner, and Z. Fakhraai, "Role of molecular layering in the enhanced mechanical properties of stable glasses," The Journal of Physical Chemistry Letters **13**, 3360–3368 (2022).
- <sup>19</sup>A. N. Raegen, J. Yin, Q. Zhou, and J. A. Forrest, "Ultrastable monodisperse polymer glass formed by physical vapour deposition," Nature materials **19**, 1110–1113 (2020).
- <sup>20</sup>M. S. Beasley, C. Bishop, B. J. Kasting, and M. D. Ediger, "Vapor-deposited ethylbenzene glasses approach "ideal glass" density," The journal of physical chemistry letters **10**, 4069–4075 (2019).
- <sup>21</sup>K. L. Kearns, S. F. Swallen, M. D. Ediger, T. Wu, Y. Sun, and L. Yu, "Hiking down the energy landscape: Progress toward the kauzmann temperature via vapor deposition," The Journal of Physical Chemistry B **112**, 4934–4942 (2008).
- <sup>22</sup>A. Gujral, K. A. O'Hara, M. F. Toney, M. L. Chabinyc, and M. Ediger, "Structural characterization of vapor-deposited glasses of an organic hole transport material with x-ray scattering," Chemistry of Materials **27**, 3341–3348 (2015).
- <sup>23</sup>C. Bishop, K. Bagchi, M. F. Toney, and M. Ediger, "Vapor deposition rate modifies anisotropic glassy structure of an anthracene-based organic semiconductor," The Journal of Chemical Physics 156, 014504 (2022).

- <sup>24</sup>K. J. Dawson, K. L. Kearns, L. Yu, W. Steffen, and M. D. Ediger, "Physical vapor deposition as a route to hidden amorphous states," Proceedings of the National Academy of Sciences **106**, 15165–15170 (2009).
- <sup>25</sup>K. Bagchi, N. E. Jackson, A. Gujral, C. Huang, M. F. Toney, L. Yu, J. J. De Pablo, and M. Ediger, "Origin of anisotropic molecular packing in vapor-deposited alq3 glasses," The Journal of Physical Chemistry Letters **10**, 164–170 (2018).
- <sup>26</sup>Z. Fakhraai, T. Still, G. Fytas, and M. Ediger, "Structural variations of an organic glassformer vapor-deposited onto a temperature gradient stage," The Journal of Physical Chemistry Letters 2, 423–427 (2011).
- <sup>27</sup>Y. Guo, A. Morozov, D. Schneider, J. W. Chung, C. Zhang, M. Waldmann, N. Yao, G. Fytas, C. B. Arnold, and R. D. Priestley, "Ultrastable nanostructured polymer glasses," Nature materials **11**, 337–343 (2012).
- <sup>28</sup>M. Tanaka, M. Auffray, H. Nakanotani, and C. Adachi, "Spontaneous formation of metastable orientation with well-organized permanent dipole moment in organic glassy films," Nature Materials **21**, 819–825 (2022).
- <sup>29</sup>T. Pérez-Castañeda, C. Rodríguez-Tinoco, J. Rodríguez-Viejo, and M. A. Ramos, "Suppression of tunneling two-level systems in ultrastable glasses of indomethacin," Proceedings of the National Academy of Sciences **111**, 11275–11280 (2014).
- <sup>30</sup>S. Singh, M. D. Ediger, and J. J. De Pablo, "Ultrastable glasses from in silico vapour deposition," Nature materials **12**, 139–144 (2013).
- <sup>31</sup>Y. Chua, M. Ahrenberg, M. Tylinski, M. Ediger, and C. Schick, "How much time is needed to form a kinetically stable glass? ac calorimetric study of vapor-deposited glasses of ethylcyclohexane," The Journal of chemical physics **142**, 054506 (2015).
- <sup>32</sup>K. L. Kearns, P. Krzyskowski, and Z. Devereaux, "Using deposition rate to increase the thermal and kinetic stability of vapor-deposited hole transport layer glasses via a simple sublimation apparatus," The Journal of Chemical Physics **146**, 203328 (2017).
- <sup>33</sup>D. Qi, Z. Fakhraai, and J. Forrest, "Substrate and chain size dependence of near surface dynamics of glassy polymers," Physical review letters 101, 096101 (2008).
- <sup>34</sup>R. R. Baglay and C. B. Roth, "Local glass transition temperature t g (z) of polystyrene next to different polymers: Hard vs. soft confinement," The Journal of Chemical Physics **146**, 203307 (2017).
- <sup>35</sup>Y. J. Gagnon and C. B. Roth, "Local glass transition temperature t g (z) within polystyrene is

- strongly impacted by the modulus of the neighboring pdms domain," ACS Macro Letters **9**, 1625–1631 (2020).
- <sup>36</sup>K. Bagchi, C. Deng, C. Bishop, Y. Li, N. E. Jackson, L. Yu, M. Toney, J. De Pablo, and M. Ediger, "Over what length scale does an inorganic substrate perturb the structure of a glassy organic semiconductor?" ACS applied materials & interfaces **12**, 26717–26726 (2020).
- <sup>37</sup>M. E. Fiori, K. Bagchi, M. F. Toney, and M. Ediger, "Surface equilibration mechanism controls the molecular packing of glassy molecular semiconductors at organic interfaces," Proceedings of the National Academy of Sciences **118**, e2111988118 (2021).
- <sup>38</sup>T. J. Ferron, M. E. Fiori, M. Ediger, D. M. DeLongchamp, and D. F. Sunday, "Composition dictates molecular orientation at the heterointerfaces of vapor-deposited glasses," JACS Au 3, 1931–1938 (2023).
- <sup>39</sup>E. D. Cubuk, R. Ivancic, S. S. Schoenholz, D. Strickland, A. Basu, Z. Davidson, J. Fontaine, J. L. Hor, Y.-R. Huang, Y. Jiang, N. C. Keim, K. D. Koshigan, J. A. Lefever, T. Liu, X.-G. Ma, D. J. Magagnosc, E. Morrow, C. P. Ortiz, J. M. Rieser, A. Shavit, T. Still, Y. Xu, Y. Zhang, K. N. Nordstrom, P. E. Arratia, R. W. Carpick, D. J. Durian, Z. Fakhraai, D. J. Jerolmack, D. Lee, J. Li, R. Riggleman, K. T. Turner, A. G. Yodh, D. S. Gianola, and A. J. Liu, "Structure-property relationships from universal signatures of plasticity in disordered solids," Science 358, 1033–1037 (2017).
- <sup>40</sup>Y. Zhang, E. C. Glor, M. Li, T. Liu, K. Wahid, W. Zhang, R. A. Riggleman, and Z. Fakhraai, "Long-range correlated dynamics in ultra-thin molecular glass films," The Journal of Chemical Physics **145**, 114502 (2016).
- <sup>41</sup>Y. Jin, A. Zhang, S. E. Wolf, S. Govind, A. R. Moore, M. Zhernenkov, G. Freychet, A. A. Shamsabadi, and Z. Fakhraai, "Glasses denser than the supercooled liquid," Proceedings of the National Academy of Sciences **118**, e2100738118 (2021).
- <sup>42</sup>D. M. Walters, R. Richert, and M. D. Ediger, "Thermal stability of vapor-deposited stable glasses of an organic semiconductor," The Journal of Chemical Physics **142**, 134504 (2015).
- <sup>43</sup>K. Paeng, S. F. Swallen, and M. Ediger, "Direct measurement of molecular motion in freestanding polystyrene thin films," Journal of the American Chemical Society **133**, 8444–8447 (2011).
- <sup>44</sup>E. Thoms, J. Gabriel, A. Guiseppi-Elie, M. Ediger, and R. Richert, "In situ observation of fast surface dynamics during the vapor-deposition of a stable organic glass," Soft Matter **16**, 10860–10864 (2020).
- <sup>45</sup>C. J. F. Böttcher and P. Bordewijk, *Theory of electric polarization*, Vol. 2 (Elsevier Science

- Limited, 1978).
- <sup>46</sup>J. Hermans, P. Hermans, D. Vermaas, and A. Weidinger, "Quantitative evaluation of orientation in cellulose fibres from the x-ray fibre diagram," Recueil des Travaux Chimiques des Pays-Bas **65**, 427–447 (1946).
- <sup>47</sup>S. S. Dalal, A. Sepúlveda, G. K. Pribil, Z. Fakhraai, and M. Ediger, "Density and birefringence of a highly stable  $\alpha$ ,  $\alpha$ ,  $\beta$ -trisnaphthylbenzene glass," The Journal of chemical physics **136**, 204501 (2012).
- <sup>48</sup>Y. Han, X. Huang, A. C. Rohrbach, and C. B. Roth, "Comparing refractive index and density changes with decreasing film thickness in thin supported films across different polymers," The Journal of Chemical Physics **153**, 044902 (2020).
- <sup>49</sup>I. Johnston, D. McCluskey, C. Tan, and M. Tracey, "Mechanical characterization of bulk sylgard 184 for microfluidics and microengineering," Journal of Micromechanics and Microengineering **24**, 035017 (2014).
- <sup>50</sup>S. Mirigian and K. S. Schweizer, "Elastically cooperative activated barrier hopping theory of relaxation in viscous fluids. i. general formulation and application to hard sphere fluids," The Journal of chemical physics **140**, 194506 (2014).
- <sup>51</sup>S. Samanta, G. Huang, G. Gao, Y. Zhang, A. Zhang, S. Wolf, C. N. Woods, Y. Jin, P. J. Walsh, and Z. Fakhraai, "Exploring the importance of surface diffusion in stability of vapor-deposited organic glasses," The Journal of Physical Chemistry B **123**, 4108–4117 (2019).
- <sup>52</sup>D. M. Ebenstein and K. J. Wahl, "A comparison of jkr-based methods to analyze quasi-static and dynamic indentation force curves," Journal of colloid and interface science **298**, 652–662 (2006).
- <sup>53</sup>E. Reedy, "Thin-coating contact mechanics with adhesion," Journal of Materials Research **21**, 2660–2668 (2006).
- <sup>54</sup>J. C. Lötters, W. Olthuis, P. H. Veltink, and P. Bergveld, "The mechanical properties of the rubber elastic polymer polydimethylsiloxane for sensor applications," Journal of micromechanics and microengineering **7**, 145 (1997).
- <sup>55</sup>J. E. Pye and C. B. Roth, "Physical aging of polymer films quenched and measured free-standing via ellipsometry: controlling stress imparted by thermal expansion mismatch between film and support," Macromolecules **46**, 9455–9463 (2013).
- <sup>56</sup>S. Dogru, B. Aksoy, H. Bayraktar, and B. E. Alaca, "Poisson's ratio of pdms thin films," Polymer Testing **69**, 375–384 (2018).

- 57"Dow chemical company, technical data sheet sylgard 184," https://www.dow.com/content/dam/dcc/documents/en-us/productdatasheet/11/11-31/11-3184-sylgard-184-elastomer.pdf, accessed on: 2023-05-17.
- <sup>58</sup>F. Schneider, J. Draheim, R. Kamberger, and U. Wallrabe, "Process and material properties of polydimethylsiloxane (pdms) for optical mems," Sensors and Actuators A: Physical **151**, 95–99 (2009).
- <sup>59</sup>D. Cai, A. Neyer, R. Kuckuk, and H. M. Heise, "Raman, mid-infrared, near-infrared and ultraviolet-visible spectroscopy of pdms silicone rubber for characterization of polymer optical waveguide materials," Journal of Molecular Structure **976**, 274–281 (2010).
- <sup>60</sup>A. Santiago-Alvarado, A. Cruz-Félix, J. González-García, O. Sánchez-López, A. Mendoza-Jasso, and I. Hernández-Castillo, "Polynomial fitting techniques applied to opto-mechanical properties of pdms sylgard 184 for given curing parameters," Materials Research Express 7, 045301 (2020).
- <sup>61</sup>"Python based package developed at the nsls-ii for giwaxs data processing," https://github.com/NSLS-II-SMI/smi-analysis, accessed on: 2023-06-11.
- 62"Foxtrot software developed by synchrotron soleil for x-ray scattering data analysis," https://www.synchrotron-soleil.fr/en/beamlines/swing, accessed on: 2023-06-11.

### **ACKNOWLEDGEMENTS**

We thank Mark D. Ediger for insightful discussions. We acknowledge financial support from the National Science Foundation (NSF) Materials Research Science and Engineering Centers (MRSEC) under grant DMR-1720530. Support during manuscript revisions and final editing was provided by Wisconsin MRSEC grant DMR-2309000. The authors acknowledge the use of the Dual Source and Environmental X-ray Scattering facility operated by the Laboratory for Research on the Structure of Matter at the University of Pennsylvania supported by NSF through DMR-2309043. This research used the 12-ID (SMI) beamline of the National Synchrotron Light Source II, a U.S. Department of Energy (DOE) Office of Science User Facility operated for the DOE Office of Science by Brookhaven National Laboratory under Contract No. DE-SC0012704. P.L. acknowledges postdoctoral fellowship funding from the School of Arts and Sciences of the University of Pennsylvania. C.Y.C acknowledges support from the NSF Graduate Research Fellowship Program (NSF GRFP, DGE-1845298).

Author Contributions: Z.F. directed the project. P.L. performed the sample preparations, AFM, SE, and in-house GIWAXS measurements with the help of S.G. and T.N.; P.L., S.E.W., D.H.K., R.B.S., C.Y.C., M.Z., and P.W. performed the synchrotron GIWAXS measurements; P.L., S.E.W., and P.W. analyzed the GIWAXS data. B.M. performed the AFM indentation experiments. P.L. and Z.F. wrote the paper with help from all authors.

Conflict of Interest: The authors have no conflict of interest to declare.